Green and solvent-free supercritical CO_2-assisted production of superparamagnetic graphene oxide aerogels: Application as superior contrast-agent in MRI

*Alejandro Borrás,[a] Julio Fraile,[a] Albert Rosado,[a] Gregorio Marbán,[b] Gerard Tobias,[a] Ana M. López-Periago,[a] Concepcion Domingo[a]**

[a] Materials Science Institute of Barcelona (ICMAB-CSIC), c/ Til.lers s/n, Campus UAB, 08193 Barcelona (Spain). *conchi@icmab.es

[b] Instituto de Ciencia y Tecnología del Carbono (INCAR-CSIC), c/ Francisco Pintado Fe 26, 33011 Oviedo (Spain).

Number of pages: 11

Number of figures: 4

Number of tables: 1

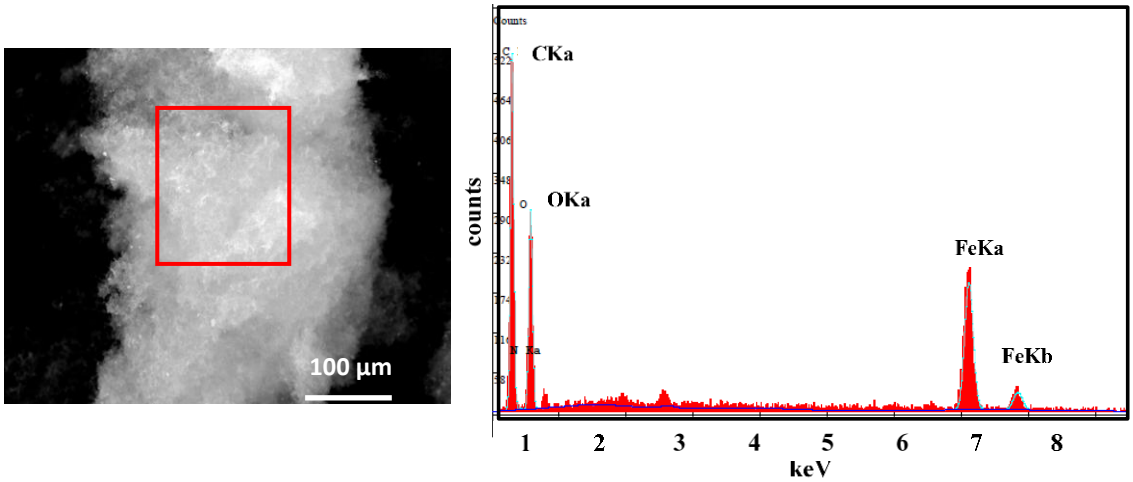

Figure S1. EDS mapping of Fe_3O_4@GO composite aerogel.

XPS calculations for the surface composition of the samples

The deconvolution procedure of the XPS data yielded the curves depicted in Figs. S2 to S5.

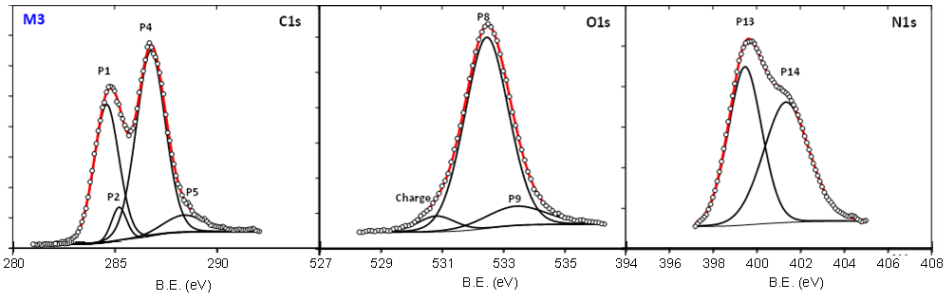

Figure S2. XPS deconvolution results for GO aerogel sample in the different spectral regions.

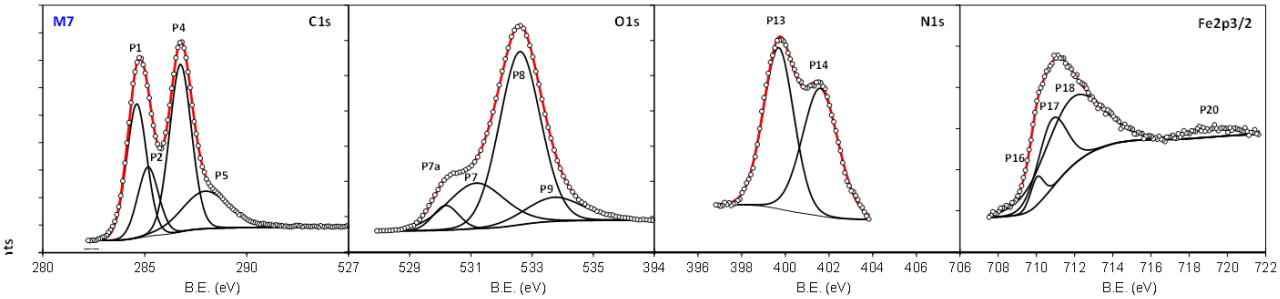

Figure S3. XPS deconvolution results for Fe_3O_4@GO composite in the different spectral regions.

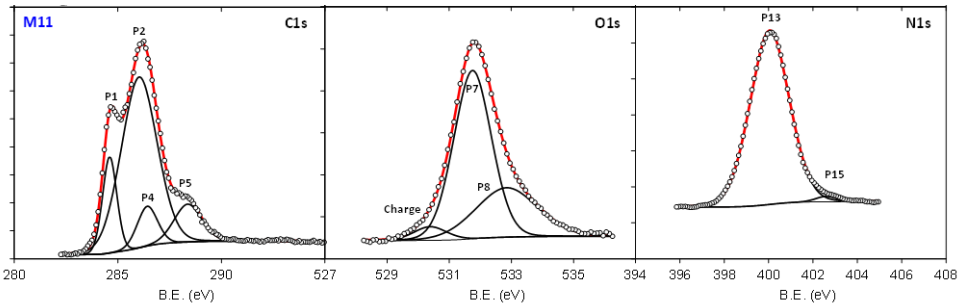

Figure S4. XPS deconvolution results for *pei*GO aerogel sample in the different spectral regions.

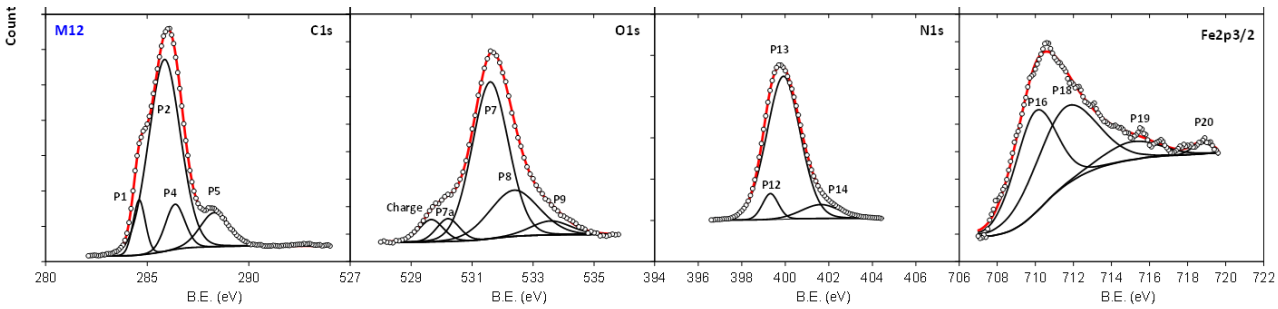

Figure S5. XPS deconvolution results for *pei*(Fe_3O_4@GO) aerogel in the different spectral regions. From spectral data, the atomic percentage for each peak was calculated and the obtained values are shown in Table S1.

Table S1. Atomic percentages (α_i) of the different analysed regions (C 1s, O 1s, N 1s, Fe 2p3/2) and correspondent peaks.

Peak	**<B.E.> [eV]**	**GO**	**Fe_3O_4@GO**	***pei*GO**	***pei*(Fe_3O_4@GO)**
C (C1s)		**65.18**	**61.01**	68.44	**67.99**
Charge	283.3	-	-	-	-
P1	284.6	22.3	16.9	10.1	5.35
P2	285.4	3.24	9.55	44.8	48.0
P4	286.6	35.1	23.1	5.92	7.00
P5	288.2	4.52	11.4	7.65	7.62
P5b	288.8	0.00	0.00	0.00	0.00
P6	290.2	0.00	0.00	0.00	0.00
O (O1s)		**33.5**	**36.0**	**11.3**	**11.4**
Charge	530.3	-	-	-	-
P7a	530.2	0.00	2.12	0.00	0.66
P7	531.4	0.00	7.73	7.65	7.16
P8	532.5	29.3	21.9	3.69	2.85
P9	535.5	4.12	4.23	0.00	0.70
P9b	534.4	0.00	0.00	0.00	0.00
N (N1s)		**1.36**	**1.20**	**20.2**	**20.0**
P12	398.9	0.00	0.00	0.00	1.45
P13	399.8	0.67	0.62	19.9	16.7
P14	401.6	0.69	0.58	0.00	1.85
P15	403.0	0.00	0.00	0.33	0.00
Fe (Fe2p3/2)		**-**	**1.80**	**-**	**0.65**
P16	710.0	-	0.10	-	0.27
P17	710.8	-	0.53	-	0.00
P18	711.7	-	1.07	-	0.30
P19	715.1	-	0.00	-	0.06
P20	719.0	-	0.11	-	0.01

As can be observed in the Figs. S2-S5, the four regions analyzed (C 1s, O 1s, N 1s, Fe 2p3/2) were correctly deconvoluted by means of around twenty peaks. The following peaks and assignations were used:

C 1s region peaks:

- *Charge* peak at **283.3** eV can be assigned either to carbide species[1] or to a charging effect,[2] though it is irrelevant for quantification purposes. In this work, it was attributed to a charging effect, and the area of the region was corrected accordingly.
- P1 at **284.6** eV is ascribed to adventitious or C=C (sp^2 bonds) carbon[3] and was used as the reference peak to correct the position of all regions.
- P2 at **285.4 ± 0.3** can be ascribed to C-H sp^3 bonds and/or carbon atoms in -C-N functional groups.[4]
- P4 at **286.6 ± 0.2** eV is ascribed to -C-O-C-, -C-OH[5] and -C=N[6] functional groups.
- P5 at **288.2 ± 0.2** eV is ascribed to >C=O[7] and O=C-O[8] groups.
- P5b at **288.8 ± 0.4** eV is ascribed to carboxylic acid groups (-COOH)[3]
- P6 at **290.2 ± 0.1** eV is ascribed here to a satellite of the C=C peak,[9] thus contributing to the carbon sp^2 together with P1.

O 1s region peaks:

- *Charge* peak at **530.3 ± 0.4** eV is ascribed to an inhomogeneous charge effect.[10]
- P7a at **530.2** eV is ascribed to FeO_x bonds.[11]
- P7 at **531.4 ± 0.2** eV is ascribed to >C=O groups[12] or Fe-OH groups.[13]
- P8 at **532.5 ± 0.2 eV** is attributed to C-OH, <u>O</u>=C-O-C=<u>O</u>, R-O-R and R-O-C=<u>O</u> groups.[3]
- P9 at **533.5 ± 0.1** eV is ascribed to oxygen in O=C-<u>O</u>-C=O and R-<u>O</u>-C=O.[3]
- P9b at **534.4 ± 0.1** eV is ascribed to oxygen in –COOH.[3]

Chemisorbed water, potentially contributing to the spectra with a peak at 535.5 eV,[14] is absent in all the samples.

N 1s region peaks:

- P12 at **398.9 ± 0.4** eV is ascribed to pyridinic nitrogen.[15]
- P13 at **399.8 ± 0.3** eV is ascribed to amine/amide functionalities.[16] Although both functionalities are considered to have a similar binding energy, most authors consider that the amines show up at a slightly lower binding energy than the amides.[17]
- P14 at **401.6 ± 0.3** eV is ascribed to graphitic nitrogen.[15]
- P15 at **403.0 ± 0.6** eV appears in an insignificant proportion in the N 1s spectra of *pei*GO and can be attributed to several causes, such as charging effects,[18] π excitations,[19] NO groups[20] or even graphitic nitrogen.[15]

Fe 2p3/2 region peaks:

- P16 at **710.0** eV is ascribed to Fe^{2+} ions in iron oxide.[21]
- P17 at **710.8** eV is ascribed to Fe^{3+} ions in iron oxide.[21]
- P18 at **711.7 ± 0.2** eV is ascribed to Fe^{3+} ions in FeOOH (goethite).[13]
- P19 at **715.1** eV is a satellite peak of Fe^{2+}.[22]
- P20 at **719.0 ± 0.3** eV is a satellite peak of Fe^{3+}.[22]

With the atomic percentages evaluated by the deconvolution procedure of each peak (α_i values, where i stands for the name of the corresponding peak) and the peak assignations above indicated, the following equations can be established (%E_F represents the atomic percentage of an element E, referred to the total amount of superficial C, O and S, that belongs to a functionality F):

$$\alpha_{P1} + \alpha_{P6} = \%C_{C=C} \quad (1)$$

$$\alpha_{P2} = \%C_{C-sp^3} + \%C_{C-N} \quad (2)$$

$$\alpha_{P4} = \%C_{C-O-C} + \%C_{C-OH} + \%C_{C=N} \quad (3)$$

$$\alpha_{P5} = \%C_{>C=O} + \%C_{R-O-\boxed{C}=O} + \%C_{O=C-O-C=O} \quad (4)$$

$$\alpha_{P5b} = \%C_{COOH} \quad (5)$$

$$\alpha_{P7} = \%C_{>C=O} + \%O_{Fe-OH} \quad (6)$$

$$\alpha_{P7a} = \%O_{Fe-O} \quad (7)$$

$$\alpha_{P8} = \%O_{C-OH} + \%O_{C-O-C} + \%O_{R-O-C=\boxed{O}} + \%O_{\boxed{O}=C-O-C=\boxed{O}} \quad (8)$$

$$\alpha_{P9} = \%O_{R-\boxed{O}-C=O} + \%O_{O=C-\boxed{O}-C=O} \quad (9)$$

$$\alpha_{P9b} = \%O_{COOH} \quad (10)$$

$$\alpha_{P10} = \%O_{H_2O} \quad (11)$$

$\alpha_{P12} = \%N_{N-pyd}$ (pyridinic nitrogen) (12)

$\alpha_{P13} = \%N_{N-ami}$ (aminic/amidic nitrogen) (13)

$\alpha_{P14} = \%N_{N-gr}$ (graphitic nitrogen) (14)

Additionally, the following restrictions can be deduced:

$$\%C_{>C=O} = \%O_{>C=O} \quad (15)$$

$$\%C_{C-OH} = \%O_{C-OH} \quad (16)$$

$$\%C_{O=C-O-C=O} = \%O_{\boxed{O}=C-O-C=\boxed{O}} \quad (17)$$

$$\%C_{R-O-\boxed{C}=O} = \%O_{R-O-C=\boxed{O}} \quad (18)$$

$$\%C_{C-O-C} = 2 \times \%O_{C-O-C} \quad (19)$$

$$\%C_{C-N} = \%N_{C-ami} \quad (20)$$

$$\%C_{C=N} = \%N_{N-pyd} + \%N_{N-gr} \quad (21)$$

$$\%O_{COOH} = 2 \times \%C_{COOH} \quad (22)$$

$$\%O_{\boxed{O}=C-O-C=\boxed{O}} = 2 \times \%O_{O=C-\boxed{O}-C=O} \quad (23)$$

$$\%O_{R-O-C=\boxed{O}} = \%O_{R-\boxed{O}-C=O} \quad (24)$$

$$\%O_{Fe-O} = \%Fe_{Fe(II)-O} + 1.5 \times \%Fe_{Fe(III)-O} + \%Fe_{FeOOH} \quad (25)$$

$$\%O_{Fe-OH} = \%Fe_{FeOOH} \quad (26)$$

With the above equations, the composition of the samples in terms of the different functionalities can be established as:

$$\%C_{C=C} = \alpha_{P1} + \alpha_{P6} \quad (27)$$

$$\%C_{C-sp^3} = \alpha_{P2} - \alpha_{P13} \quad (28)$$

$$\%C_{C-N} = \alpha_{P13} \quad (29)$$

$$\%C_{C=N} = \alpha_{P12} + \alpha_{P14} \quad (30)$$

$$\%C_{C-O-C} = 2 \times [\alpha_{P4} - \alpha_{P8} + \alpha_{P5} - \alpha_{P7} + \alpha_{P18} - \alpha_{P12} - \alpha_{P14}] \quad (31)$$

$$\%C_{C-OH} = 2 \times [\alpha_{P8} - \alpha_{P5} + \alpha_{P7} - \alpha_{P18}] + \alpha_{P12} + \alpha_{P14} - \alpha_{P4} \quad (32)$$

$$\%C_{>C=O} = \alpha_{P7} - \alpha_{P18} \quad (33)$$

$$\%C_{R-O-\boxed{C}=O} = 2 \times \alpha_{P9} - \alpha_{P5} + \alpha_{P7} - \alpha_{P18} \quad (34)$$

$$\%C_{O=C-O-C=O} = 2 \times [\alpha_{P5} - \alpha_{P7} + \alpha_{P18} - \alpha_{P9}] \quad (35)$$

$$\%C_{COOH} = \alpha_{P5b} = 0.5 \times \alpha_{P9b} \quad (36)$$

$$\%N_{N-ami} = \alpha_{P13} \quad (37)$$

$$\%N_{N-pyd} = \alpha_{P12} \quad (38)$$

$$\%N_{N-gr} = \alpha_{P14} \quad (39)$$

$$\%Fe_{FeOOH} = \alpha_{P18} \quad (40)$$

$$\%Fe_{Fe(II)-O} = \alpha_{P16} + \alpha_{P19} \quad (41)$$

$$\%Fe_{Fe(III)-O} = \alpha_{P17} + \alpha_{P20} \quad (42)$$

The deconvolutions of C 1s and O 1s regions were performed simultaneously by home-made *ad hoc* Microsoft® Excel macros in order to minimize an error function that simultaneously excluded negative values of the different functional group percentages (eqs. (27) to (42)) and permitted to fulfil the balances expressed by equations (22) and (25). The results of applying equations (27) to (42) to the values indicated in Table S1 are shown in Table 1 (main text), where the surface composition of the different samples is established.

REFERENCES

1. Dontas, I.; Kennou, S. The interfacial properties of erbium films on the two polar faces of 6H-SiC (0001). *Diam. Relat. Mater.* **2001**, 10, 13-17. DOI: 10.1016/S0925-9635(00)00359-9.
2. Titirici, M. M.; Thomas, A.; Yu, S. H.; Muller, J. O.; Antonietti, M. A Direct Synthesis of mesoporous carbons with bicontinuous pore morphology from crude plant material by hydrothermal carbonization. *Chem. Mater.* **2007**, 19, 4205-4212. DOI: 10.1021/cm0707408.
3. Chiang, Y-C.; Chen, Y-J.; Wu, C-Y. Effect of relative humidity on adsorption breakthrough of CO_2 on activated carbon fibers. *Materials* **2017**, 10, 1296. DOI: 10.3390/ma10111296. DOI: 10.3390/ma10111296.
4. Briggs, D.; Beamson, G. Primary and secondary oxygen-induced C1s binding energy shifts in X-ray photoelectron spectroscopy of polymers. *Anal. Chem.* **1992**, 64, 1729-1736. DOI: 10.1021/ac00039a018.
5. Han, P.; Yue, Y.; Liu, Z.; Xu, W.; Zhang, L.; Xu, H.; Dong, S.; Cui, G. Graphene oxide nanosheets/multi-walled carbon nanotubes hybrid as an excellent electrocatalytic material towards VO^{2+}/VO_2^{+} redox couples for vanadium redox flow batteries. *Energy Environ. Sci.* **2011**, 4, 4710-4717. DOI: 10.1039/C1EE01776D.
6. Indrawirawan, S.; Sun, H.; Duan, X.; Wang, S. Low temperature combustion synthesis of nitrogen-doped graphene for metal-free catalytic oxidation, *J. Mater. Chem.* A **2015**, 3, 3432-3440. DOI: 10.1039/C4TA05940A.
7. Huang, Y-L.; Tien, H-W.; Ma, C-C. M.; Yang, S-Y.; Wu, S-Y.; Liu, H-Y.; Mai, Y-W. Effect of extended polymer chains on properties of transparent graphene nanosheets conductive film. *J. Mater. Chem.* **2011**, 21, 18236-18241. DOI: 10.1039/C1JM13790E.

8. Ou, J.; Zhang, Y.; Chen, L.; Zhao, Q.; Meng, Y.; Guo, Y.; Xiao, D. Nitrogen-rich porous carbon derived from biomass as a high performance anode material for lithium ion batteries. *J. Mater. Chem. A* **2015**, 3, 6534-6541. DOI: 10.1039/C4TA06614F
9. Buchner, F.; Forster-Tonigold, K.; Bozorgchenani, M.; Gross, A.; Behm, R.J. Interaction of a self-assembled ionic liquid layer with graphite(0001): A combined experimental and theoretical study. *J. Phys. Chem. Lett.* **2016**, 7, 226-233. DOI: 10.1021/acs.jpclett.5b02449.
10. Massey, S.; Roy, D.; Adnot, A. Study of natural ageing of polypropylene by X-ray photoelectron spectroscopy. *Nuc. Inst. Meth. Phys. Res. B: Beam Inter. Mater. Atoms* **2003**, 208, 236-241. DOI: 10.1016/S0168-583X(03)00662-1.
11. Allen, G. C.; Curtis, M. T.; Hooper, A. J.; Tucker, P. M. X-Ray photoelectron spectroscopy of iron–oxygen systems. *Dalton Trans.* **1974**, 1525-1530. DOI: 10.1039/DT9740001525
12. Darmstadt, H.; Roy, C.; Kaliaguine, S. ESCA characterization of commercial carbon-blacks and of carbon-blacks from vacuum pyrolysis of used tires. *Carbon* **1994**, 32, 1399-1406. DOI: 10.1016/0008-6223(94)90132-5.
13. Teterin, Y. A.; Kalmykov, S. N.; Novikov, A. P.; Sapozhnikov, Y. A.; Vukchevich, L.; Teterin, A. Y. U.; Maslakov, K. I.; Utkin, I. O.; Hasanova, I. B.; Shcherbina, N. S. X-ray photoelectron spectroscopy study of interaction of Np^{5+} with goethite α-FeOOH. *Nuc. Tech. Rad. Protec.* 2005, 20, 38-44. DOI: 10.2298/NTRP0501038T.
14. Puziy, A. M.; Poddubnaya, O. I.; Socha, R. P.; Gurgul, J.; Wisniewski, M. XPS and NMR studies of phosphoric acid activated carbons. *Carbon* **2008**, 46, 2113-2123. DOI: 10.1016/j.carbon.2008.09.010.
15. Scardamaglia, M.; Susi, T.; Struzzi, C.; Snyders, R.; Di Santo, G.; Petaccia, L.; Bittencourt, C. Spectroscopic observation of oxygen dissociation on nitrogen-doped graphene. *Sci. Reports* **2017**, 7, 7960. DOI: 10.1038/s41598-017-08651-1.

16. Jansen, R. J. J.; van Bekkum, H. XPS of nitrogen-containing functional groups on activated carbon. *Carbon* **1995**, 33, 1021-1027. DOI: 10.1016/0008-6223(95)00030-H.

17. Compton, O. C.; Dikin, D. A.; Putz, K. W.; Brinson, L. C.; Nguyen, S. T. Electrically conductive "alkylated" graphene paper via chemical reduction of amine-functionalized graphene oxide paper. *Adv. Mater.* **2010**, 22, 892-896. DOI: 10.1002/adma.200902069.

18. Thomas, A.; Fischer, A.; Goettmann, F.; Antonietti, M.; Muller, J-O.; Schlogl, R.; Carlsson, J. M. Graphitic carbon nitride materials: variation of structure and morphology and their use as metal-free catalysts. *J. Mater. Chem.* **2008**, 18, 4893-4908. DOI: 10.1039/B800274F

19. Guo, Q.; Xie, Y.; Wang, X.; Zhang, S.; Hou, T.; Lv, S. Synthesis of carbon nitride nanotubes with the C_3N_4 stoichiometry via a benzene-thermal process at low temperatures. *Chem. Commun.* **2004**, 26-27. DOI: 10.1039/B311390F.

20. Favaro, M.; Carraro, F.; Cattelan, M.; Colazzo, L.; Durante, C.; Sambi, M.; Gennaro, A.; Agnoli, S.; Granozzi, G. Multiple doping of graphene oxide foams and quantum dots: new switchable systems for oxygen reduction and water remediation. *J. Mater. Chem. A* **2015**, 3, 14334-14347. DOI: /10.1039/C5TA01561H.

21. Ke, S.; Lin, P.; Zeng, X.; Huang, H.; Zhou, L. M.; Mai, Y. W. Tuning of dielectric and ferroelectric properties in single phase $BiFeO_3$ ceramics with controlled Fe^{2+}/Fe^{3+} ratio. *Ceram. Inter.* **2014**, 40, 5263-5268. DOI: 10.1016/j.ceramint.2013.10.098.

22. Shaharyar, Y.; Cheng, J. Y.; Han, E.; Maron, A.; Weaver, J.; Marcial, J.; McCloy, J. S.; Goel, A. Elucidating the effect of iron speciation (Fe^{2+}/Fe^{3+}) on crystallization kinetics of sodium aluminosilicate glasses. *J. Am. Cer. Soc.* **2016**, 99 2306-2315. DOI: 10.1111/jace.14239